Enhanced piezoelectricity in twinned ferroelastics with nanocavities

Guangming Lu,[1,2] Suzhi Li,[1,*] Xiangdong Ding,[1,†] Jun Sun,[1] and Ekhard K. H. Salje[1,2,‡]
[1]*State Key Laboratory for Mechanical Behavior of Materials, Xi'an Jiaotong University, Xi'an 710049, China*
[2]*Department of Earth Sciences, University of Cambridge, Cambridge CB2 3EQ, United Kingdom*

(Received 31 May 2020; accepted 30 June 2020; published 17 July 2020)

Enhancing the electromechanical response by engineering domain boundaries in multiferroics has become a highly active research field in recent years. The starting point is the discovery that ferroelastic twin walls are polar inside a nonpolar matrix. The density of such twin walls is then greatly enhanced by forming complex twin patterns. Our computer simulations show that the interaction of nanocavities with differently charged configurations with twin boundaries generates strong piezoelectricity in ferroelastic (nonferroelectric) crystals. Cavity-induced domain patterns statistically break the inversion symmetry of a sample even when the cavities themselves obey inversion symmetry with relatively weak emerging piezoelectricity ($d \sim 10^{-3}$ pm/V) . Stronger piezoelectricity occurs in noncentrosymmetric charged cavity arrangements with a coefficient of $d \sim 10^{-1}$pm/V. Structurally, the electric field polarizes and shifts the nanocavities by the displacement of trapped surface charges. The related strain fields interact with the ferroelastic domains, which act as soft bridges between the nanocavities. This leads to a significant deformation of the entire sample and hence to enhanced piezoelectricity. Our simulation results point to new directions for designing and enhancing electromechanical nanodevices based on ferroelastic templates even when the bulk material is structurally centrosymmetric.

DOI: 10.1103/PhysRevMaterials.4.074410

I. INTRODUCTION

Experimentally, piezoelectricity has been shown to depend on a multitude of geometrical factors, such as the grain size in SiO_2 based compounds [1], domain size of ferroelectrics [2] and local structural heterogeneity of rare-earth-doped $Pb(Mg_{1/3}Nb_{2/3})O_3 - PbTiO_3$ (PMN − PT) [3]. Pieoelectricity was observed in incommensurate phases, paraelectric $BaTiO_3$ near the transition point and nonpoled relaxor ferroelectrics [4,5]. All these macroscopic pieozelectric effects can be classified as "spurious" because the macroscopic samples are statistically centrosymmetric and detailed investigations are needed to identify the exact origin of piezoelectricity in each case. The statistically inhomogeneous responses can be activated either by designing the shapes of the nanocrystals [6] or constructing compositionally graded structures [7]. In a different scenario, structural interfaces [8–11] inside ferroelastic materials break the centro-symmetry. Twin walls between different ferroelastic twin variants are typically polar [12–23]. The polarity stems either from flexoelectricity near twin walls or from biquadratic coupling between polarization and strain [15,24–26]. The density of polar elements can be massively enhanced in tweed structures [27,28] or in a complex twin pattern [29,30]. Under the framework of the domain boundary engineering [31], the functional properties could be controlled by manipulating the compositions, densities or positions of the domain walls. Local ferroelastic patches under piezoelectric force microscopy (PFM) tips are observed to be piezoelectric while the overall effect vanishes due to the cancelation by space averaging. In addition, the complex ferroelastic structures have been reported to show weak piezoelectricity ($d \sim 10^{-4}$ pm/V) [32].

To further enhance the overall piezoelectric effect, we may induce large local inhomogeneous strain by making twin walls to interact with other structural defects, such as vacancies [33], dislocations [34] and voids [35–37]. Among all the defects, nanoscale cavities are the preferred candidates to strongly affect the formation of twin patterns since cavities act as preferential sites to generate twin walls inside ferroelastic domains. Porosity in ferroelastic and coelastic materials can be very high [35], particularly in minerals and SiO_2 based materials. Such nanocavities can be the consequence of radiation damage [38–41] or patterning by focused ion beam (FIB) milling [42]. Unlike metals, diffusion leading to rearrangements of nanocavities is usually very slow in minerals and even very old minerals maintain the initial arrangements over billions of years. Experimentally, ferroelectric walls in $KTiOPO_4$ have been previously injected by periodically arranged cavities [42]. Their piezoelectric effect and their relations with various domain patterns were never investigated.

Here we concentrate on the possible enhancement of piezoelectric effect by interacting nanocavities with ferroelastic twin walls. The cavities are of nanoscale size and periodically or randomly distributed inside the ferroelastic domain in our atomistic simulations. One key element of cavity generated nanostructures is the state of the surface charge inside the cavities. External surfaces can be easily neutralized by free electrons or moving charged defects [43–47]. In case of cavities this mechanism may not be appropriate because the cavity is created by destroying different atomic bonds that could be

*Corresponding author: lisuzhi@xjtu.edu.cn
†Corresponding author: dingxd@mail.xjtu.edu.cn
‡Corresponding author: ekhard@esc.cam.ac.uk

the sinks of hydrion [48,49] forming new chemical bounds to compensate the excess charges near the inner surfaces. This mechanism would form charge-free surfaces in cavities. However, in some other cases, where the system is hydrion-deficient, such compensation would not occur and the cavity surfaces are charged. Another important aspect relates to the distribution of nanocavities inside the matrix. The randomly distributed cavities are commonly observed in nature or when the materials are subjected to radiation damage, while periodically arranged cavities can be generated by FIB milling [42]. We structure the paper according to these two commonly used techniques. Under each scenario, we mimic different inner surface states where the surfaces of the nanocavities are charged or charge-free by breaking chemical bonds either along charge compensated directions or randomly. We found that weak piezoelectricity ($d \sim 10^{-3}$ pm/V) occurs in charge-free nanocavities while strong piezoelectricity ($d \sim 10^{-1}$ pm/V) follows from the direct interactions between the external electric field and charges on the nanocavity surfaces.

II. ATOMIC MODEL

Our simulations are based on a two-dimensional toy model with two base atoms carrying negative charges (A atom) and positive charges (B atom) [30]. The ferroelastic twins (A sublattice) are constructed by using double-well Landau springs with a shear angle of 2°. The atomic interactions between cations, and cations and anions are purely harmonic to exclude any additional polar instability in the bulk. The polarity condenses only inside the twin walls where the inversion symmetry is broken by the change of the shear angle across the walls and the flexoelectric relaxation. The model parameters are inspired by $SrTiO_3$ with the energy scale determined by $T_c = 105$ K and a typical ferroelastic shear angle of 2° [12]. All model parameters are listed in Table SI in the Supplemental Material [50].

To exclude the piezoelectric responses from the sample surfaces, periodic boundary conditions were implemented in both the x-[10] and y-[01] directions. Thus, any piezoelectricity measured in our simulations are entirely ascribed to polar structures like twin walls, kinks, and junctions [21,30,51]. We introduced nanocavities into the monodomain either periodically or randomly. The periodically distributed cavities mimic the resulting functional template of the ferroic materials that are engineered by means of FIB milling. The randomly distributed cavities mimic porous materials in nature or when the material is subjected to radiation damage. The surfaces of cavities were either charged or charge-free. The charge-free configuration possesses surface layers with an equal number of A and B atoms. For the charged surfaces, four different electrostatic states of the inner cavity surfaces were considered, i.e., entirely negative surfaces with excess A atoms at the surfaces of a round cavity, quadrupolar surfaces with negative and positives charges segments, dipolar surfaces with four different surface configurations (dipole vectors along the [11], [1–1], [-11] and [-1-1] directions) and dipolar surfaces with fixed charge distributions (dipole vectors along the [11] direction). A complex twin pattern was obtained by applying two-directional shear to the monodomain sample. The large-scale atomic/molecular massively parallel simulator (LAMMPS) [52] was used to simulate ferroelastic twin structures. The simulations maintain the number of particles, temperature and pressure, i.e., the isothermal-isobaric ensemble [53].

The polar displacement in each unit cell is determined by the relative displacement of the anion with respect to the central position of its four cation neighbors. Polar displacements are very large near the cavity surfaces due to the loss of bonds. The averaged polarization density of the entire systems is calculated as $\langle P\rangle = qs/V$, where $q(= 1.6 \times 10^{-19}$ C) is the electron charge, $\langle s\rangle^2 = \sqrt{\langle s_x\rangle^2 + \langle s_y\rangle^2}$ is the averaged polar displacements, and V is the system volume. We define two parameters to characterize the electromechanical coupling [32]. The piezoelectric coefficients are $d_{ijk} = \frac{\partial \varepsilon(E)_{ij}}{\partial E_k}$ ($i,\ j = 1, 2$ and $k = 1, 2$) at constant stress, where $\varepsilon(E)$ is the field induced strain and E is the electrical field. The electrostrictive parameters are $Q_{ijkl} = \frac{\partial^2 \varepsilon(P)_{ij}}{\partial \langle P\rangle_k \partial \langle P_l\rangle}$ ($i,\ j = 1,\ 2$ and $k,\ l = 1, 2$), where $\varepsilon(P)$ is the field induced strain and $\langle P\rangle$ is the averaged polarization density. The piezoelectric coefficients are determined by fitting $\varepsilon(E)$ curves and the electrostrictive coefficients are determined by fitting $\varepsilon(P)$ curves. The calibration of the ferroelastic monodomain with inversion symmetry showed no piezoelectric effect within a noise level of $\sim 10^{-5}$ pm/V.

III. RESULTS AND DISCUSSION

Starting from a ferroelastic monodomain [Fig. 1(a)], nanocavities were introduced either in a periodic distribution corresponding to FIB milling [Fig. 1(b)] or in a random distribution corresponding to radiation damage [Fig. 1(c)]. Shear strains were then applied to generate a complex domain pattern. The electromechanical response was finally investigated under an external electrical field [Figs. 1(d) and 1(e)]. We consider the inner surfaces of the nanocavities with four different states of charge, as charge-free surfaces with an equal number of A and B atoms at four {11} planes [Fig. 2(a)], negatively charged surfaces with excess A atoms at the surfaces of a round cavity [Fig. 2(b)], quadrupolar surfaces with half excess A atoms and half excess B atoms at the surfaces of a round cavity [Fig. 2(c)] and dipolar surfaces with excess A atoms on two {10} surfaces and excess cation B atoms on the other {10} surfaces [Fig. 2(d)].

A. Piezoelectricity inside the ferroelastic domains induced by periodically arranged nanocavities

Twin boundaries show a local electromechanical response underneath a PFM tip [28]. This response lacks spatial correlations and does not induce collective displacements, which are required for actuator applications. Furthermore, the charge distributions at the inner surfaces dominate the macroscopic deformation of the sample [54]. Collectively controlling the polar ferroelastic twin walls for different charge configurations is hence the key for applications. In this section, we explore the different electrostatic states of nanoscale cavities inside ferroelastics using atomistic simulations (see Atomic Model Section and Supplemental Material Table SI [50]). The distribution of the nanocavities are first arranged to be periodic to mimic the resulting domain patterns engineered by FIB milling. Ferroelastic twin walls are then injected around

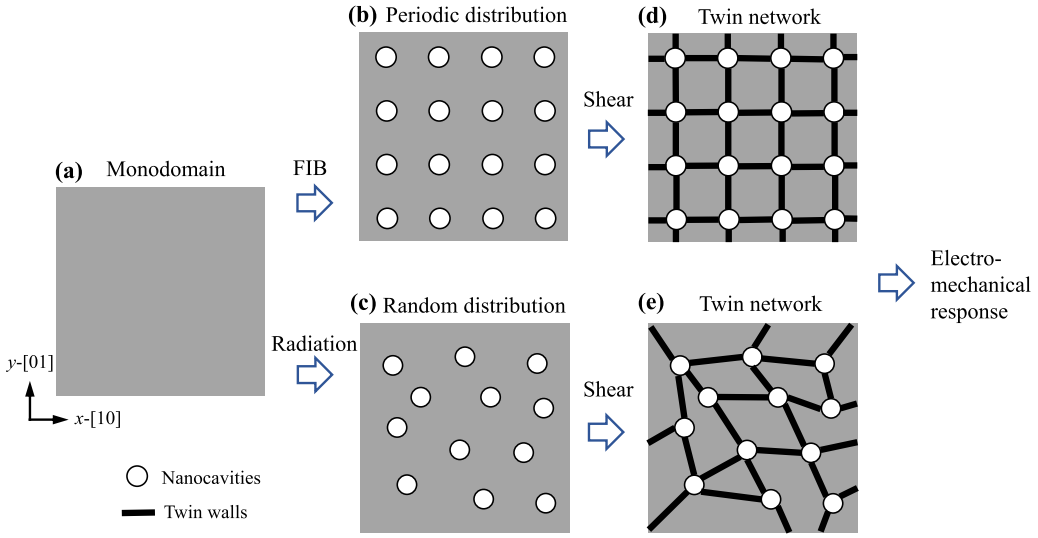

FIG. 1. Schematic illustration of construction of twinned ferroelastics with nanocavities. (a) the ferroelastic monodomain sample. Introduction of nanocavities with either (b) for a periodic distribution of nanocavities by FIB milling or (c) a random distribution corresponding to radiation damage. (d) and (e) Two-dimensional shear strain was then applied to generate a domain network for each case. The electromechanical response was finally investigated under an external electrical field.

nanocavities into the systems by mechanical deformation. The electromechanical responses of the different systems are finally characterized. For comparison, we futher studied the electromechancial response for a monodomain and a highly complex twin pattern in the absence of nanocavities (see Supplemental Material Figs. S1 and S2 and Table SII [50]).

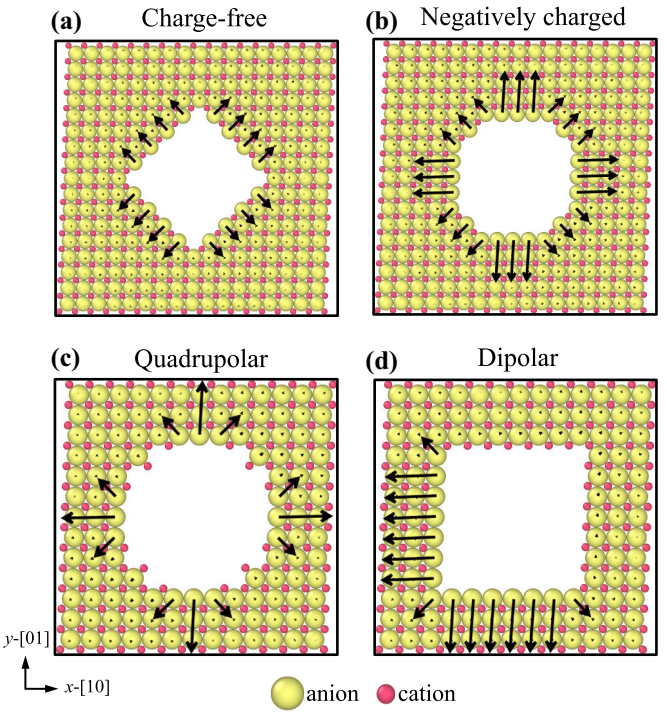

FIG. 2. Nanocavities with (a) charge-free surfaces with an equal number of A and B atoms at four {11} planes, (b) negatively charged surfaces with excess A atoms at the surfaces of a round cavity, (c) quadrupolar surfaces with half A atoms and half B atoms at the surfaces of a circular cavity, and (d) dipolar surfaces with excess A atoms on two {10} surfaces and excess cation B atoms on the other {10} surfaces.

1. Charge-free cavities

We first mimic the experimental FIB technique to generate periodic, charge-free nanocavities in a $100a \times 100a$ monodomain, which a is lattice unit length of 0.1 nm. The nanocavities are arranged inside the monodomain with separations of 2.5 nm (Fig. 3, Fig. S3 [50]). The nanocavities are cut in square shape with no excess net charges at the surface layers, i.e., an equal number of cations and anions [55] (see details in Fig. 2(a) and Supplemental Material Fig. S3 [50]). Large electric dipoles appear on the inner surfaces due to breaking of atomic bonds (Figs. S3b, S3e [50]). Additional dipoles appear near cavities with nonuniform strain fields (Fig. S3c [50]). Each cavity breaks the local inversion symmetry, but the overall pattern obeys the macroscopic inversion symmetry. We then applied an external electric field along the x-[10] direction to check the electromechanical response. Inhomogeneous strains were observed locally near cavities under the electric field [Fig. 3(b)]. The electric field induced strains throughout the entire monodomain shows pure electrostriction with $Q \sim 10^{-8}\text{cm}^4/\mu\text{C}^2$. No piezoelectricity is observed [Fig. 3(e)]. Furthermore, two dimensional shear along the x-[10] and y-[01] directions was applied to the monodomain in order to generate a complex domain pattern. These nanocavities inside the monodomain act as nucleation sites for ferroelastic twin walls. They inject polar twin walls by forming ferroelastic domain patterns with twin walls linking the cavities [Fig. 3(c)]. The cavities and the linking twin walls are a source of inhomogeneous strain under an external electric field [Fig. 3(d)]. With this complex microstructure, we observed a significant piezoelectric response with the piezoelectric coefficient $d \sim -4.47 \times 10^{-4}$ pm/V under an electric field along the x-[10] direction [Fig. 1(e)]. The

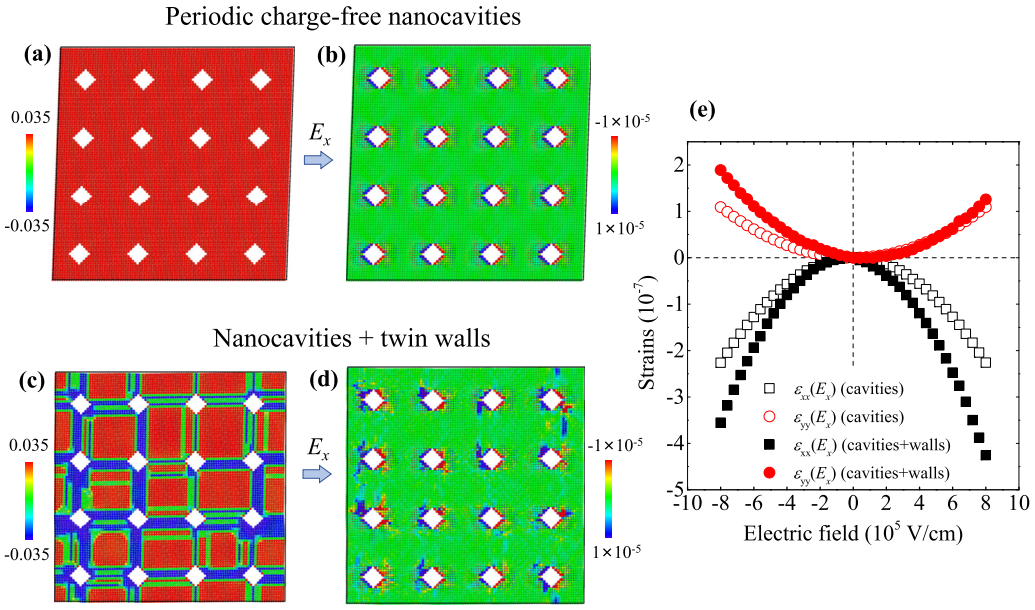

FIG. 3. Comparison of the electromechanical behavior of a ferroelastic monodomain containing periodic charge-free nanocavities with and without a network of twins. (a) The atomic configuration of a ferroelastic monodomain with a periodic distribution of charge-free nanocavities. The colors are coded according to the atomic-level shear strain (ε_{xy}). ε_{xy} is calculated as the shear strain with respect to the unsheared state. (b) The response of normal strain under the electrical field along the x-[10] direction E_x. The colors are coded according to the atomic-level normal strain (ε_{xx}). ε_{xx} is calculated as the strain with respect to the state without electrical field. (c) A complex twin network is further generated by shearing along two directions x-[10] and y-[01]. The colors are coded according to the atomic-level shear strain (ε_{xy}). (d) The response of normal strain under the same electrical field in twining network with nanocavities. The colors are coded according to the atomic-level normal strain (ε_{xx}). (e) Dependence of the macroscopic strains $\varepsilon_{xx}(E_x)$ and $\varepsilon_{yy}(E_x)$ on E_x in two systems. The system containing periodic charge-free nanocavities show an electrostrictive effect with $Q \sim 10^{-8}\,\mathrm{cm}^4/\mu\mathrm{C}^2$. Weak piezoelectricity with $d \sim -4.47 \times 10^{-4}\,\mathrm{pm/V}$ is observed after introducing the twin network due to inhomogeneous strain near the twin walls.

relevant results for the electric field applied along the y-[01] direction are shown in the Supplemental Material (see Fig. S4 and Table SIII [50]).

In comparison to the systems in the absence of nanocavities, a monodomain was created with an equilibrium shear angle of 2° (Fig. S1 [50]). A complex twin pattern with a dense array of twin walls is generated by applying shear in two orthogonal directions (horizontal and vertical), as shown in Fig. S1c [50]. The twin walls are polar via the flexoelectric effect [12]. Many kinks (steps in the twin wall) and junctions (intersections of two oriented twin walls) appear in complex twin patterns. The kinks and junctions carry net polarities due to the breaking of macroscopic inversion symmetry. Although the local polarization near these structural defects is large (Fig. S1d [50]), the averaged polarization of the cavity sample is very small with $\langle P_x \rangle = -1.08 \times 10^{-4}\,\mathrm{mC/cm}^2$, $\langle P_y \rangle = 1.7 \times 10^{-5}\,\mathrm{mC/cm}^2$. We then explore the coupling between electric polarization and strain in both monodomain and complex twin patterns under an external electric field. Figure S4 [50] shows the variation of macroscopic strain components $(\varepsilon_{xx}(E), \varepsilon_{yy}(E))$ as a function of the applied electric field along the x-[10] and y-[01] directions. The monodomain is purely electrostrictive with $Q \sim 10^{-8}\mathrm{cm}^4/\mu\mathrm{C}^2$ (no piezoelectricity) while an additional weak piezoelectric response ($d \sim 1.32 \times 10^{-4}\,\mathrm{pm/V}$) is observed in the complex twin pattern (see Table SII in the Supplemental Material [50]), in accordance with our earlier studies [32]. Such weak piezoelectricity inside the complex twins can be ascribed to polar ferroelastic twin walls, and the cancellation of polarity with different wall directions. However, different from the nonengineered complex twin structure, the space averaging inside the cavity-controlled twinning networks is effectively decreased. Therefore, the piezoelectric coefficient for the cavity-induced twin network is found to be around four times larger than that of the cavity-free complex twin pattern.

2. *Charged cavities*

We now change the surface charge states of nanocavities [Figs. 2(b)–2(d)]. We first investigate the negatively charged nanocavities. The cavities are introduced in round shape with negative atomic layers (A atoms) attached to the inner surfaces (see Fig. 2(b) and Supplemental Material Fig. S5 [50]). We observed the large surface dipoles together with dipoles induced by the inhomogeneous strains near the nanocavities [Fig. 4(a)]. Different from the charge-free surfaces, the negative charges are trapped at the surfaces and interact with the external electric field. Atomic layers near the nanocavities are shifted by the external electric field with large field induced strain [Fig. 4(b)]. The local strain cannot induce macroscopic piezoelectricity due to the restrictions of the overall inversion symmetry of the sample, but shows significant electrostriction with $Q \sim 10^{-8}\,\mathrm{cm}^4/\mu\mathrm{C}^2$ [Fig. 4(e)]. Ferroelastic twin walls are then injected by external shear strains [Fig. 4(c)]. The generated ferroelastic twins form a network, which lowers the statistical possibility of polarization compensation. The

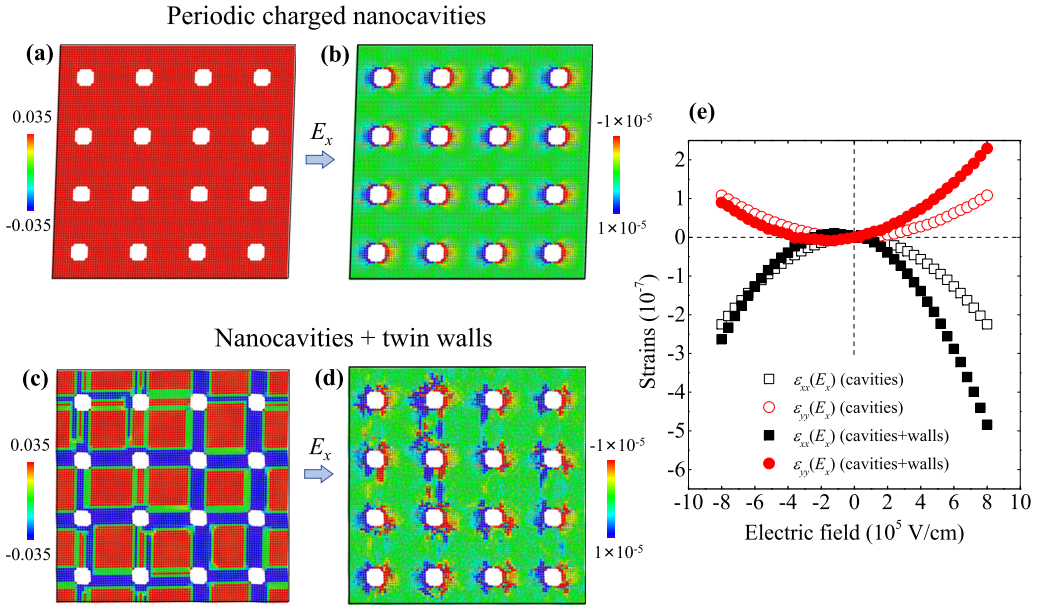

FIG. 4. Comparison of the electromechanical behavior of a ferroelastic monodomain containing periodic, negatively charged nanocavities with and without a twinning network. (a) The atomic configuration of a ferroelastic monodomain with periodic distribution of negatively charged nanocavities. The colors are coded according to the atomic-level shear strain (ε_{xy}). ε_{xy} is calculated as the shear strain with respect to the unsheared state. (b) The response of normal strain under the electrical field E_x along x-[10]. The colors are coded according to the atomic-level normal strain (ε_{xx}). ε_{xx} is calculated as the strain with respect to the state without electrical field. (c) A complex twinning network is generated by shear along x-[10] and y-[01]. The colors are coded according to the atomic-level shear strain (ε_{xy}). (d) The response of normal strain under the same electrical field in twining network with nanocavities. The colors are coded according to the atomic-level normal strain (ε_{xx}). (e) The dependence of macroscopic strains $\varepsilon_{xx}(E_x)$ and $\varepsilon_{yy}(E_x)$ under E_x in two systems. The system containing periodic negatively charged nanocavities show an electrostrictive effect with $Q \sim 10^{-8}\,\mathrm{cm}^4/\mu\mathrm{C}^2$. Additional piezoelectricity $d \sim -1.33 \times 10^{-3}\,\mathrm{pm/V}$ is observed after introducing a twin network. The value of the piezoelectric coefficient is enhanced by one order of magnitude in comparison with Fig. 3(e).

net polarization for a twin-wall network is $\langle P_x \rangle = 2.32 \times 10^{-2}\,\mathrm{mC/cm}^2$, $\langle P_y \rangle = 1.82 \times 10^{-3}\,\mathrm{mC/cm}^2$. The piezoelectric response is enhanced due to trapped charges interacting with the external electric field. The field displaces the atoms at the cavity surfaces and induces large local strains [Fig. 4(d)], which then interact with the network of elastically soft polar twin boundaries [22]. This network then extends strains to the entire ferroelastic sample inducing large macroscopic deformations. The corresponding piezoelectric coefficient is $d \sim -1.33 \times 10^{-3}\,\mathrm{pm/V}$ under an electric field along x-[10] [Fig. 4(e)]. The strain responses for a field applied along the y-[01] direction are shown in Fig. S6 and Table SIV in the Supplemental Material [50].

We then change the electrostatic properties of the nanocavities to be quadrupolar [see Figs. 2(c) and S7 [50]). The net charge of the whole surfaces is zero while containing positive and negative charged segments. Periodically arranged nanocavities are centrosymmetric (Fig. S7 [50]). The local strain near the surfaces of nanocavity (Fig. S8 [50]) is weaker than that of the negatively charged surfaces (Fig. 4 and Fig. S6 [50]). The monodomain sample with quadrupolar nanocavities shows an electrostrictive effect with $Q \sim 10^{-8}\,\mathrm{cm}^4/\mu\mathrm{C}^2$ but no piezoelectricity. With injected ferroelastic twin networks (Fig. S7d [50]), the surface charges interact with the external electric field and transmit local strains through the entire sample, inducing a detectable piezoelectric response of $d \sim 1.01 \times 10^{-3}\,\mathrm{pm/V}$. More information on the piezoelectric and electrostrictive effect under the electric fields in x-[10] and y-[01] are shown in Fig. S8 and Table SV in the Supplemental Material [50].

We finally construct the nanocavities to be dipolar. The nanocavities contain two positively charged {10} surfaces and two negatively charged {10} surfaces. The nanocavities contain dipolar vectors with four equivalently different orientations of [11], [1–1], [−11], and [-1-1] (see details in Supplemental Material Fig. S9 [50]). Nanocavities with all four different dipolar charge distributions were arranged to comply with the macroscopic inversion symmetry of the monodomain (Fig. S9 [50]). The macroscopic field induced strains are purely parabolic with $Q \sim 10^{-8}\mathrm{cm}^4/\mu\mathrm{C}^2$ (Fig. S10 [50]). Local inhomogeneous strain is located near cavities (Fig. S10 [50]) due to strong interactions between surface charges and the external electric field (Fig. S10 [50]). In comparison with the previous two models, the piezoelectric coefficient increases with $d \sim s - 4.98 \times 10^{-3}\,\mathrm{pm/V}$. The local inhomogeneous strain is massively enhanced when the dipole vectors of nanocavities are aligned along the same [11] direction (Fig. S11 and Fig. S12 [50]). The monodomain sample without twin walls has no inversion symmetry (Fig. S12a [50]) and shows strong piezoelectricity with $d \sim 2.50 \times 10^{-2}\,\mathrm{pm/V}$ caused by the large inhomogeneous strain near the nanocavities. The piezoelectricity is further increased when the ferroelastic twin walls are injected by shear stress. The piezoelectric coefficient of the twinned samples reaches $d \sim 4.48 \times 10^{-2}\,\mathrm{pm/V}$. More information on the piezoelectric and electrostrictive effect under the electric fields in x-[10]

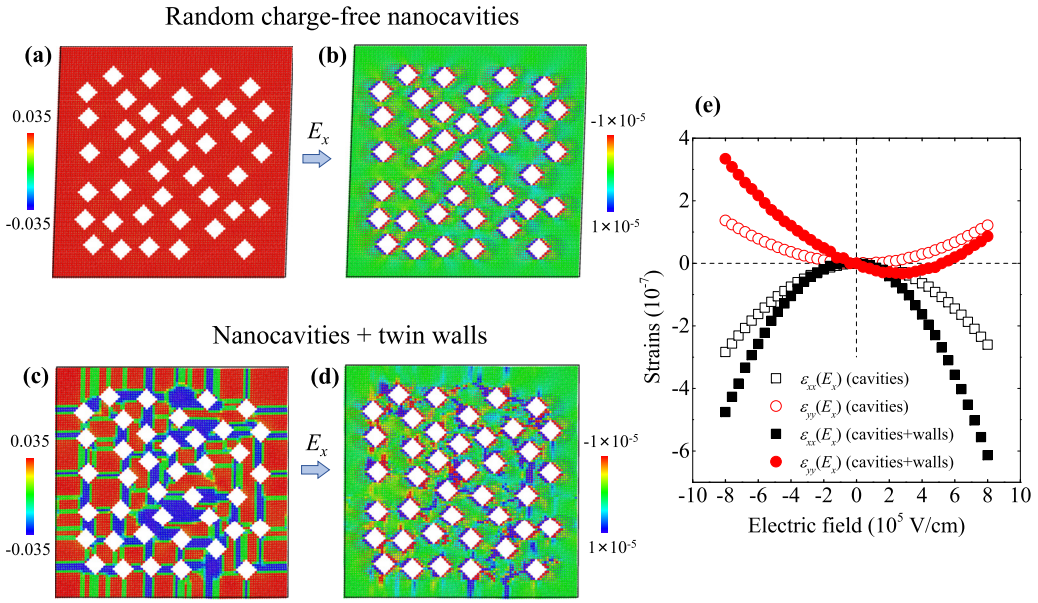

FIG. 5. Comparison of the electromechanical behavior of a ferroelastic monodomain containing random charge-free nanocavities with and without a network of twins. (a) Atomic configuration of a ferroelastic monodomain with periodic distribution of charge-free nanocavities. The colors are coded according to the atomic-level shear strain (ε_{xy}). (b) Response of normal strains under an electric field E_x. The colors are coded according to the atomic-level normal strain (ε_{xx}). (c) A complex twinning network is generated by shear along x-[10] and y-[01]. The colors are coded according to the atomic-level shear strain (ε_{xy}). (d) Response of normal strain under the same electrical field in twin networks with nanocavities. The colors are coded according to the atomic-level normal strain (ε_{xx}). (e) Dependence of macroscopic strains $\varepsilon_{xx}(E_x)$ and $\varepsilon_{yy}(E_x)$ under E_x in two systems. The randomly distributed nanocavities break the macroscopic inversion symmetry, inducing weak piezoelectricity $d \sim 1.47 \times 10^{-4}$ pm/V. The piezoelectric effect becomes stronger with $d \sim -1.64 \times 10^{-3}$ pm/V after introducing a twin network.

and y-[01] are shown in Table SVI and SVII in the Supplemental Material [50].

B. Piezoelectricity inside ferroelastic domains induced by randomly distributed nanocavities

Radiation damaging technique also generate high porosity in ferroic materials. Compared with the periodically designed patterns, the radiation damage generates randomly distributed nanocavities. The electrostatic configurations and the corresponding electromechanical properties of the nanocavities are not well investigated. Next we study the possible piezoelectric effect in twinned ferroelastic domains with randomly distributed nanocavities.

1. Charge-free cavities

We first introduced 40 charge-free nanocavities randomly distributed inside a monodomain (Figs. 5(a) and Supplemental Material Fig. S13a [50]). The size and shape of the nanocavities are the same as that in the periodic pattern [Fig. 3(a)]. The average distance between the nanocavities is smaller due to a higher density of nanocavities. The randomness of the nanocavities breaks the inversion symmetry with $\langle P_x \rangle = -8.68 \times 10^{-4}$ mC/cm^2, $\langle P_y \rangle = -2.36 \times 10^{-4}$mC/cm^2. Weak piezoelectricity ($d \sim 1.47 \times 10^{-4}$ pm/V) appears under an applied x-[10] electric field [Figs. 5(b) and 5(e)]. The macroscopic symmetry is further broken by generating a ferroelastic twin network [Fig. 5(c)] with the averaged polarization density of $\langle P_x \rangle = -1.45 \times 10^{-2}$ mC/cm^2, $\langle P_y \rangle = -1.94 \times 10^{-2}$ mC/cm^2 [Figs. 5(d) and 5(e)]. The high density of the charge-free nanocavities produces more inmogeneous strain under external electric fields. Compared with the periodic patterns in Fig. 3, a strong piezoelectric response is induced with $d \sim -8.1 \times 10^{-4}$ pm/V. The strain response for the field applied along y-[01] is shown in Supplemental Material (see Fig. S14 and Table SIII for more information [50]).

2. Charged cavities

Randomly distributed charged nanocavities with different electrostatic states of the inner surfaces break the macroscopic inversion symmetry (see Supplemental Material [50]). Inhomogeneous strains under external electric field arise from two effects: the intrinsic symmetry breaking by the randomness of the nanocavities and the strong interaction between trapped charges and the external electric field. The latter plays a dominant role in generating piezoelectricity. The piezoelectric coefficients are $d \sim 8.56 \times 10^{-4}$ pm/V for negatively charged nanocavities (Figs. 6(a) and 6(b), Fig. S15-S16 [50]), $d \sim 8.92 \times 10^{-4}$ pm/V for quadrupolar nanocavities (Figs. S17 and S18 [50]), $d \sim -1.55 \times 10^{-3}$ pm/V for dipolar nanocavities with net polar directions along four differently ⟨11⟩ directions (Figs. S19 and S20 [50]), and $d \sim 8.22 \times 10^{-2}$ pm/V for dipolar nanocavities with a fixed polar direction (Figs. S21 and S22 [50]) under an applied x-[10] electrical field. Piezoelectricity is further enhanced when ferroelastic twins are injected under shear deformation. The ferroelastic twin network becomes denser than that of periodic pattern due to more nucleation sites for twin walls. Under an external field applied along x-[10], the

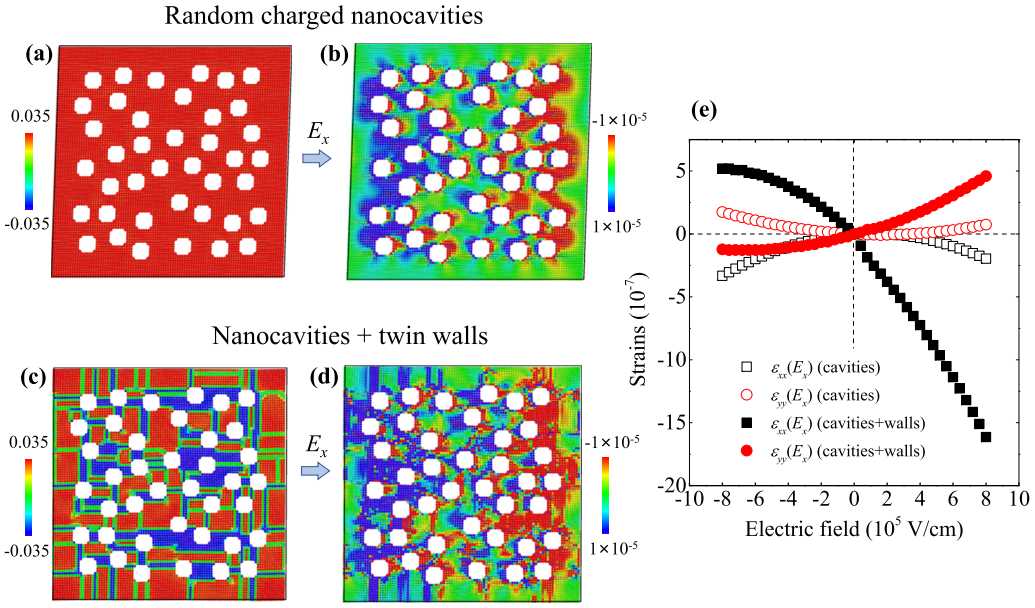

FIG. 6. Comparison of electromechanical behavior of a ferroelastic monodomain containing random, negatively charged nanocavities with and without a twinning network. (a) Atomic configuration of a ferroelastic monodomain with periodic distribution of negatively charged nanocavities. The colors are coded according to the atomic-level shear strain (ε_{xy}). (b) The response of normal strain under the electrical field E_x. The colors are coded according to the atomic-level normal strain (ε_{xx}). (c) A complex twinning network is generated by shearing along x-[10] and y-[01]. The colors are coded according to the atomic-level shear strain (ε_{xy}). (d) Response of normal strains under the same electrical field in a twin network with nanocavities. The colors are coded according to the atomic-level normal strain (ε_{xx}). (e) The dependence of macroscopic strains $\varepsilon_{xx}(E_x)$ and $\varepsilon_{yy}(E_x)$ under E_x in two systems. The system containing random negatively charged nanocavities show weak piezoelectricity with $d \sim 8.56 \times 10^{-4}$ pm/V. The piezoelectric effect is enhanced to $d \sim -1.35 \times 10^{-2}$pm/V when twin walls are injected.

corresponding piezoelectric coefficients d for the four models above are $\sim -1.35 \times 10^{-2}$ pm/V (Figs. 6(c) and 6(d), Figs. S15 and S16 [50]), $\sim 1.05 \times 10^{-2}$ pm/V (Figs. S17 and S18 [50]), $\sim -7.10 \times 10^{-3}$ pm/V (Figs. S19 and S20 [50]), and ∼0.167 pm/V (Figs. S21 and S22 [50]), respectively. The corresponding strain components and piezoelectric coefficients induced by the external electric field along the y-[01] direction are shown in Figs. S15–S22 and Table SIV–SVII in the Supplemental Material [50].

The physical origin of the enhanced piezoelectricity inside the ferroelastic domain patterns arises from two parts. The external electric field displaces the excess charges trapped on the inner surfaces, inducing large inhomogeneous strains near the cavities. They interact with ferroelastic twin walls, which are elastically softer than the bulk. Without twin walls, the local strains would remain uncorrelated. The nucleation of the ferroelastic domain walls can be engineered by the nanocavities under external shear, forming twin networks that can effectively interact with the nanocavities and transmit the local strains to the macroscopic scale. Engineered twin networks by the nanocavities act as soft bridge, which takes an importance role on enhancing piezoelectric responses of ferroelastic domains (see schematic illustration in Fig. 7). The piezoelectric coefficient for nonengineered twin walls are in the order of 10^{-4} pm/V while such effects can be engineered to increase to $\sim 10^{-1}$ pm/V for the dipolar inner surfaces. The piezoelectric and electrostrictive coefficients of various twin networks induced by periodically and randomly distributed nanocavities were shown in Fig. 8 and Table I.

C. Experimental support for enhanced piezoelectricity in porous materials

Charged domain walls have shown a strong piezoelectric response under an external electric field in multiferroic materials. Sluka *et al.* [56] found that the internal field can be controlled by the density of charged domain walls in $BaTiO_3$. It interacts with small polydomains, inducing an appreciable enhancement of the piezoelectric response. Li *et al.* [57] ascribed the enhancement of the piezoelectric response by the charged domain walls in $BaTiO_3$ and PZT due to their energetically weaker stabilities under external stress. Charged vacancies [58] enhance the electromechanical response inside AlN thin films. Some other charged interfaces exist between various soft-hard' multilayer stacks [59,60] in response to external fields. They possess excellent piezoelectric properties. The introduction of cavities goes one step further. The electromechanical properties were widely investigated in 3-1 type porous $0.94Bi_{0.5}Na_{0.5}TiO_3 - 0.06\ BaTiO_3$ (BNT-6BT) ceramic, which shows an enhanced piezoelectricity (182 pC/N) and large electric-induced strain (593 pm/V) [61]. Effects of porosity [62], shape [63], size [64], distributions [65–67], and geometric connectivity [68,69] on the piezoelectric and dielectric properties of the ceramics were tailored to obtain the biggest piezoelectric effect. Smaller nanopores instead of the micropores have been successfully fabricated using various techniques. The piezoelectric response by such nanopores has been characterized and various reasons behind the enhanced piezoelectricity have been discussed [70–74]. Nevertheless, the electrostatic properties of nanopores and

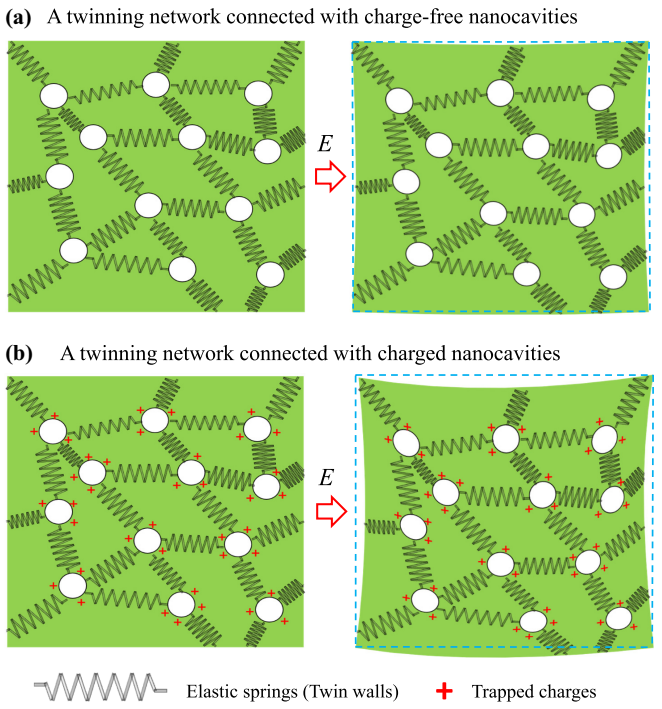

FIG. 7. Schematic illustration of the role of charged states of nanocavities and twin networks on enhancing piezoelectricity. The twin walls act as "softer springs" connecting nanocavities. They propagate inhomogeneous strain. (a) For the charge-free nanocavities, weak piezoelectricity is induced. (b) For the charged nanocavities, the trapped charges on the inner surfaces of the nanocavities react with the external electric field with larger atomic displacements, inducing large inhomogeneous strain near the cavities, inducing stronger macroscopic sample deformations and piezoelectricity.

their potential contributions to the macroscopic electromechanical response are more complex. The effect of charges on the inner surfaces of the cavities plays an important role on enhancing piezoelectricity in some cellular polymers

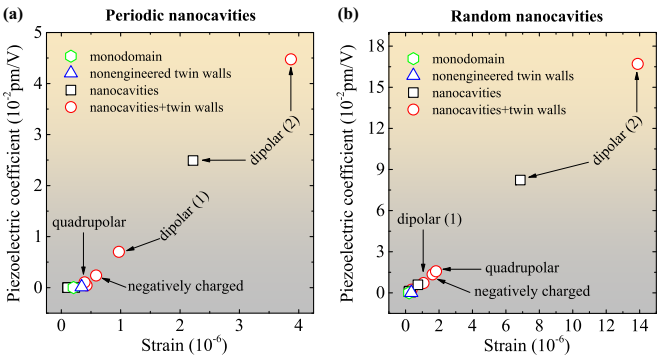

FIG. 8. Comparison of macroscopic strains and piezoelectric coefficients for ferroelastic twinning with (a) periodically and (b) randomly distributed nanocavities under an external electric field. The piezeoelectric effect is strongly related to the charge states of nanocavities. The maximum piezoelectric effect is reached with $d \sim 10^{-2}$ pm/V when the inner surfaces of nanocavities are dipolar. Piezoelectricity can be further enhanced by twin networks. Dipolar (1) nanocavities have net polar directions along four differently ⟨11⟩. Dipolar (2) nanocavities have a fixed net polar direction along [11].

[54,75–80], which can be internally charged within the voids of the polymer foam. The negatively and positively charged voids are connected by springs with different force constants, and piezoelectricity becomes a manifestation of the difference in the force constants of the springs connecting the charged voids [54]. Our observations follow a similar mechanism. The nanopores with different electrostatics were fabricated in different ferroelastic domains. The ferroelastic twin walls, acting as soft-bridges between charged cavities, were injected into the ferroelastics by external shear. The ferroelastics twin walls play a similar role as the springs with different force constants in cellular polymers under external stimulus. Our investigations on ferroelastics functionalize the trapped charges and ferroelastic twin walls as entities, and open a route for exploring and engineering the functional properties inside the ferroelastic templates.

TABLE I. Piezoelectric and electrostrictive coefficients of ferroelastic domains containing nanocavities with different charge states of surfaces.

		Piezoelectric coefficients (10^{-3} pm/V)		Electrostrictive coefficients (10^{-8} cm$^4/\mu$C^2)	
Electrostatic states	Ferroelastic patterns	d_{111}	d_{221}	Q_{1111}	Q_{2211}
No cavity (Fig. S2)	Nonengineered walls	0.132	−0.122	−2.85	1.44
Charge-free (Fig. 3,5)	Periodic cavities + walls	−0.447	−0.394	−3.49	1.40
	Random cavities + walls	−0.81	−1.64	−5.36	2.10
Negatively charged (Fig. 4,6)	Periodic cavities + walls	−1.33	0.854	−3.51	1.48
	Random cavities + walls	−13.5	3.61	−5.36	1.85
Quadrupolar (Fig. S8, S18)	Periodic cavities + walls	1.007	0.867	−3.22	1.24
	Random cavities + walls	10.48	0.698	−4.91	2.47
Dipolar (1) (Fig. S10, S20)	Periodic cavities + walls	−4.98	−0.924	−3.35	1.43
	Random cavities + walls	−7.10	5.92	−4.77	1.65
Dipolar (2) (Fig. S12, S22)	Periodic cavities + walls	44.75	−2.02	−3.19	1.28
	Random cavities + walls	167.0	−26.91	−4.55	1.50

IV. CONCLUSION

The piezoelectric effect observed in this paper is based on the role played by inhomogeneous strains. Such inhomogeneous strains are located in regions near charge-free nanocavities or charged nanocavities where strong inhomogeneous strains exist due to the interactions between trapped charges and external electric fields. External shear generates ferroelastic twin networks, which connect the cavities and act as the soft elastic links between the nanocavities. The twin network plays a key role in transmitting local inhomogeneous strains throughout the entire sample, inducing an increased macroscopic deformations of charge-free nanocavities and massively enhancing piezoelectricity for charged nanocavities. The maximum piezoelectric coefficient reached in this study is $d \sim 10^{-1}$ pm/V.

ACKNOWLEDGMENTS

X.D. and J.S. are grateful to NSFC (Grants No. 51320105014 and No. 51621063) and to the 111 project (BP 2018008) for financial support. E.K.H.S. is grateful to EPSRC (Grant No. EP/P024904/1) for support. S.L. appreciates the support from the NKRDPC (Grant No. 2019YFA0307900).

[1] J. Aufort, O. Aktas, M. A. Carpenter, and E. K. H. Salje, Am. Miner. **100**, 1165 (2015).
[2] R. Ahluwalia, T. Lookman, A. Saxena, and W. Cao, Phys. Rev. B **72**, 014112 (2005).
[3] F. Li, D. Lin, Z. Chen, Z. Cheng, J. Wang, C. Li, Z. Xu, Q. Huang, X. Liao, L.-Q. Chen, T. R. Shrout, and S. Zhang, Nat. Mater. **17**, 349 (2018).
[4] O. Aktas and E. K. H. Salje, Appl. Phys. Lett. **113**, 202901 (2018).
[5] O. Aktas, J. R. Duclère, S. Quignon, G. Trolliard, and E. K. H. Salje, Appl. Phys. Lett. **113**, 032901 (2018).
[6] A. Biancoli, C. M. Fancher, J. L. Jones, and D. Damjanovic, Nat. Mater. **14**, 224 (2015).
[7] J. Karthik, R. V. K. Mangalam, J. C. Agar, and L. W. Martin, Phys. Rev. B **87**, 024111 (2013).
[8] D. D. Viehland and E. K. H. Salje, Adv. Phys. **63**, 267 (2014).
[9] S. Van Aert, S. Turner, R. Delville, D. Schryvers, G. Van Tendeloo, X. Ding, and E. K. H. Salje, Phase Transit **86**, 1052 (2013).
[10] S. A. Hayward, J. Chrosch, E. K. Salje, and M. A. Carpenter, Eur. J. Mineral. **8**, 1301 (1997).
[11] J. Chrosch and E. K. H. Salje, J. Appl. Phys. **85**, 722 (1999).
[12] S. Van Aert, S. Turner, R. Delville, D. Schryvers, G. Van Tendeloo, and E. K. H. Salje, Adv. Mater. **24**, 523 (2012).
[13] L. Goncalves-Ferreira, S. A. T. Redfern, E. Artacho, and E. K. H. Salje, Phys. Rev. Lett. **101**, 097602 (2008).
[14] E. K. H. Salje, O. Aktas, M. A. Carpenter, V. V. Laguta, and J. F. Scott, Phys. Rev. Lett. **111**, 247603 (2013).
[15] H. Yokota, H. Usami, R. Haumont, P. Hicher, J. Kaneshiro, E. K. H. Salje, and Y. Uesu, Phys. Rev. B **89**, 144109 (2014).
[16] G. F. Nataf, M. Guennou, J. Kreisel, P. Hicher, R. Haumont, O. Aktas, E. K. H. Salje, L. Tortech, C. Mathieu, D. Martinotti, and N. Barrett, Phys. Rev. Mater. **1**, 074410 (2017).
[17] A. S. Yurkov and A. K. Tagantsev, Appl. Phys. Lett. **108**, 022904 (2016).
[18] Y. Frenkel, N. Haham, Y. Shperber, C. Bell, Y. Xie, Z. Chen, Y. Hikita, H. Y. Hwang, E. K. H. Salje, and B. Kalisky, Nat. Mater. **16**, 1203 (2017).
[19] J. F. Scott, E. K. H. Salje, and M. A. Carpenter, Phys. Rev. Lett. **109**, 187601 (2012).
[20] P. Barone, D. Di Sante, and S. Picozzi, Phys. Rev. B **89**, 144104 (2014).
[21] E. K. H. Salje, S. Li, Z. Zhao, P. Gumbsch, and X. Ding, Appl. Phys. Lett. **106**, 212907 (2015).
[22] L. Goncalves-Ferreira, S. A. T. Redfern, E. Atacho, and E. K. H. Salje, Appl. Phys. Lett. **94**, 081903 (2009).
[23] G. Lu, S. Li, X. Ding, J. Sun, and E. K. H. Salje, Phys. Rev. Mater. **3**, 114405 (2019).
[24] B. Houchmandzadeh, J. Lajzerowicz, and E. Salje, J. Phys.: Condens. Matter **3**, 5163 (1991).
[25] H. Pöttker and E. K. H. Salje, J. Phys.: Condens. Matter **26**, 342201 (2014).
[26] S. Conti, S. Müller, A. Poliakovsky, and E. K. H. Salje, J. Phys.: Condens. Matter **23**, 142203 (2011).
[27] X. Wang, E. K. H. Salje, J. Sun, and X. Ding, Appl. Phys. Lett. **112**, 012901 (2018).
[28] E. K. H. Salje, M. Alexe, S. Kustov, M. C. Weber, J. Schiemer, G. F. Nataf, and J. Kreisel, Sci. Rep. **6**, 27193 (2016).
[29] R. J. Harrison, S. A. T. Redfern, and E. K. H. Salje, Phys. Rev. B **69**, 144101 (2004).
[30] E. K. H. Salje, S. Li, M. Stengel, P. Gumbsch, and X. Ding, Phys. Rev. B **94**, 024114 (2016).
[31] E. K. H. Salje, Phase Transit. **86**, 2 (2013).
[32] G. Lu, S. Li, X. Ding, and E. K. H. Salje, Appl. Phys. Lett. **114**, 202901 (2019).
[33] X. He, S. Li, X. Ding, J. Sun, S. M. Selbach, and E. K. H. Salje, Acta Mater. **178**, 26 (2019).
[34] F. R. Estrada, L. G. M. de Moraes, F. L. A. Vital, M. D. Neme, P. Schio, T. J. A. Mori, and J. C. Cezar, Ferroelectrics **545**, 39 (2019).
[35] E. K. H. Salje, Am. Miner. **100**, 343 (2015).
[36] Y. Zhang, P. Chu, Y. L. Xie, D. P. Chen, Z. B. Yan, and J. M. Liu, EPL **108**, 27009 (2014).
[37] S. Li, Y. Li, Y.-C. Lo, T. Neeraj, R. Srinivasan, X. Ding, J. Sun, L. Qi, P. Gumbsch, and J. Li, Int. J. Plast. **74**, 175 (2015).
[38] Y. Roh, L. Trombetta, and J. Stathis, Microelectron. Eng. **22**, 227 (1993).
[39] G. Kramberger, V. Cindro, I. Mandić, M. Mikuž, and M. Zavrtanik, Nucl. Instrum. Meth. A **476**, 645 (2002).
[40] I. Pintilie, G. Lindstroem, A. Junkes, and E. Fretwurst, Nucl. Instrum. Meth. A **611**, 52 (2009).
[41] H. Zhu, M. Qin, R. Aughterson, T. Wei, G. Lumpkin, Y. Ma, and H. Li, Acta Mater. **172**, 72 (2019).
[42] J. R. Whyte, R. G. P. McQuaid, P. Sharma, C. Canalias, J. F. Scott, A. Gruverman, and J. M. Gregg, Adv. Mater. **26**, 293 (2014).
[43] K. Garrity, A. Kakekhani, A. Kolpak, and S. Ismail-Beigi, Phys. Rev. B **88**, 045401 (2013).

[44] G. Geneste and B. Dkhil, Phys. Rev. B **79**, 235420 (2009).
[45] S. V. Levchenko and A. M. Rappe, Phys. Rev. Lett. **100**, 256101 (2008).
[46] P. Maksymovych, S. Jesse, P. Yu, R. Ramesh, A. P. Baddorf, and S. V. Kalinin, Science **324**, 1421 (2009).
[47] Y. Yun and E. I. Altman, J. Am. Chem. Soc. **129**, 15684 (2007).
[48] K. J. Alvine, M. Vijayakumar, M. E. Bowden, A. L. Schemer-Kohrn, and S. G. Pitman, J. Appl. Phys. **112**, 043511 (2012).
[49] K. Heinola and T. Ahlgren, J. Appl. Phys. **107**, 113531 (2010).
[50] See Supplemental Material at http://link.aps.org/supplemental/10.1103/PhysRevMaterials.4.074410 for additional information on the results of strain maps and ε-E curves for various systems.
[51] L. Zhang, S. Li, X. Ding, J. Sun, and E. K. Salje, Appl. Phys. Lett. **116**, 102902 (2020).
[52] S. Plimpton, J. Comput. Phys. **117**, 1 (1995).
[53] M. Parrinello and A. Rahman, J. Appl. Phys. **52**, 7182 (1981).
[54] M. Wegener and S. Bauer, ChemPhysChem **6**, 1014 (2005).
[55] G. Lu, S. Li, X. Ding, J. Sun, and E. K. H. Salje, Sci. Rep. **9**, 15834 (2019).
[56] T. Sluka, A. K. Tagantsev, D. Damjanovic, M. Gureev, and N. Setter, Nat. Commun. **3**, 748 (2012).
[57] Z. Li, H. Wu, and W. Cao, J. Appl. Phys. **111**, 024106 (2012).
[58] N. Sharma, M. Rath, S. Ilango, T. R. Ravindran, M. S. R. Rao, S. Dash, and A. K. Tyagi, J. Phys. D: Appl. Phys. **50**, 015601 (2017).
[59] R. Gerhard-Multhaupt, X. Zhengfu, W. Kunstler, and A. Pucher, Preliminary study of multi-layer space-charge electrets with piezoelectric properties from porous and nonporous Teflon films, in *10th International Symposium on Electrets* (*ISE 10*) (IEEE, New York, 1999), pp. 273.
[60] G. S. Neugschwandtner, R. Schwödiauer, S. Bauer-Gogonea, and S. Bauer, Appl. Phys. A **70**, 1 (2000).
[61] S. Zhu, L. Cao, Z. Xiong, C. Lu, and Z. Gao, J. Eur. Ceram. Soc. **38**, 2251 (2018).
[62] A.-K. Yang, C.-A. Wang, R. Guo, and Y. Huang, Appl. Phys. Lett. **98**, 152904 (2011).
[63] S. Iyer and T. A. Venkatesh, J. Appl. Phys. **110**, 034109 (2011).
[64] R. Guo, C.-A. Wang, and A. Yang, J. Eur. Ceram. Soc. **31**, 605 (2011).
[65] Z. Li, C. Wang, and C. Chen, Comput. Mater. Sci. **27**, 381 (2003).
[66] R. Kar-Gupta and T. A. Venkatesh, Acta Mater. **54**, 4063 (2006).
[67] R. Kar-Gupta and T. A. Venkatesh, Appl. Phys. Lett. **91**, 062904 (2007).
[68] H. Wang, G. Tan, S. Cen, and Z. Yao, Eng. Anal. Bound. Elem. **29**, 636 (2005).
[69] S. Iyer and T. A. Venkatesh, Appl. Phys. Lett. **97**, 072904 (2010).
[70] R. Kar-Gupta and T. A. Venkatesh, Acta Mater. **56**, 3810 (2008).
[71] E. Stava, M. Yu, H. C. Shin, H. Shin, D. J. Kreft, and R. H. Blick, Lab Chip **13**, 156 (2013).
[72] A. Castro, P. Ferreira, B. J. Rodriguez, and P. M. Vilarinho, J. Mater. Chem. C **3**, 1035 (2015).
[73] P. Ferreira, R. Z. Hou, A. Wu, M.-G. Willinger, P. M. Vilarinho, J. Mosa, C. Laberty-Robert, C. Boissière, D. Grosso, and C. Sanchez, Langmuir **28**, 2944 (2012).
[74] L. H. He, Appl. Phys. Lett. **88**, 151909 (2006).
[75] X. Zhang, J. Huang, J. Chen, Z. Wan, S. Wang, and Z. Xia, Appl. Phys. Lett. **91**, 182901 (2007).
[76] M. Wegener, W. Wirges, and B. Tiersch, J. Porous Mater. **14**, 111 (2007).
[77] X. Qiu, J. Appl. Phys. **108**, 011101 (2010).
[78] G. S. Neugschwandtner, R. Schwödiauer, M. Vieytes, S. Bauer-Gogonea, S. Bauer, J. Hillenbrand, R. Kressmann, G. M. Sessler, M. Paajanen, and J. Lekkala, Appl. Phys. Lett. **77**, 3827 (2000).
[79] M. Lindner, H. Hoislbauer, R. Schwodiauer, S. Bauer-Gogonea, and S. Bauer, IEEE Trans. Dielectr. Electr. Insul. **11**, 255 (2004).
[80] P. Fang, X. Qiu, W. Wirges, R. Gerhard, and L. Zirkel, IEEE Trans. Dielectr. Electr. Insul. **17**, 1079 (2010).